Title

EFFECT OF PROLONGED HIGH-TEMPERATURE EXPOSURE ON THE FATIGUE AND FRACTURE BEHAVIOR OF ALUMINUM-LITHIUM ALLOY 2090

Authors

Venkateswara, K.T.
Ritchie, R.O.

Publication Date

1987-06-01

LBL-23126
Preprint

Center for Advanced Materials

CAM REPORT

Submitted to Materials Science and Engineering

Effect of Prolonged High-Temperature Exposure on the Fatigue and Fracture Behavior of Aluminum-Lithium Alloy 2090

K.T. Venkateswara Rao and R.O. Ritchie

June 1987

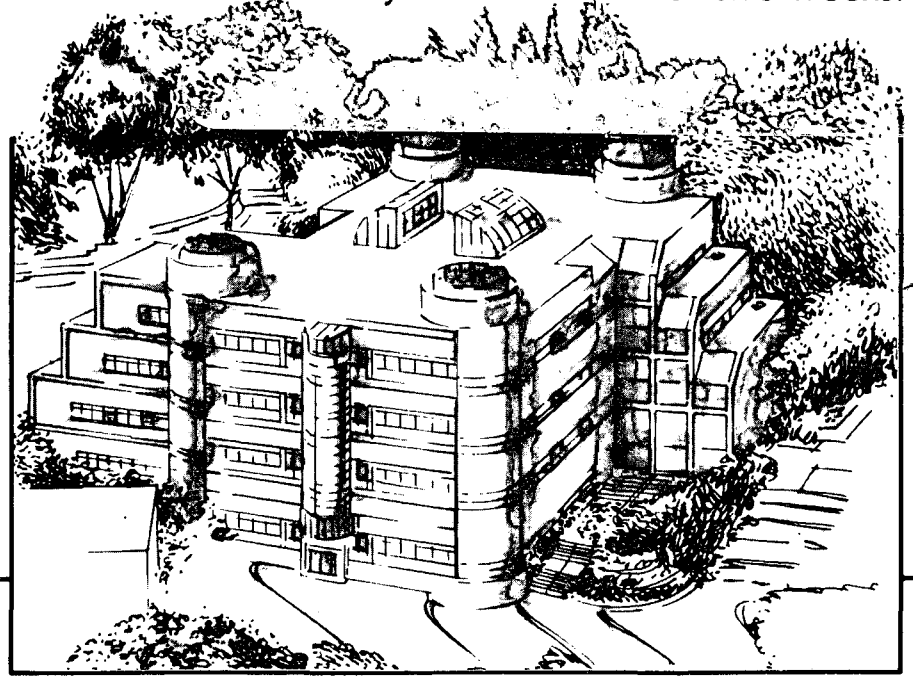

Materials and Chemical Sciences Division

Lawrence Berkeley Laboratory • University of California

ONE CYCLOTRON ROAD, BERKELEY, CA 94720 • (415) 486-4755

Prepared for the U.S. Department of Energy under Contract DE-AC03-76SF00098

DISCLAIMER

LBL-23126

EFFECT OF PROLONGED HIGH-TEMPERATURE EXPOSURE ON THE FATIGUE AND FRACTURE BEHAVIOR OF ALUMINUM-LITHIUM ALLOY 2090

K. T. Venkateswara Rao and R. O. Ritchie

Center for Advanced Materials, Lawrence Berkeley Laboratory, and
Department of Materials Science and Mineral Engineering,
University of California, Berkeley, CA 94720

March 1987

submitted to Materials Science and Engineering

This work was supported by the Director, Office of Energy Research, Office of Basic Energy Sciences, Materials Sciences Division of the U.S. Department of Energy under Contract No. DE-AC03-76SF00098.

EFFECT OF PROLONGED HIGH-TEMPERATURE EXPOSURE ON THE FATIGUE AND FRACTURE BEHAVIOR OF ALUMINUM-LITHIUM ALLOY 2090

K. T. Venkateswara Rao and R. O. Ritchie

Center for Advanced Materials, Lawrence Berkeley Laboratory, and
Department of Materials Science and Mineral Engineering,
University of California, Berkeley, CA 94720 (U.S.A.)

ABSTRACT

Effects of prolonged exposures of 100 to 1000 hours at 163°C on fatigue crack propagation and fracture toughness behavior have been studied in commercial aluminum-lithium alloy 2090-T8E41, and results compared with behavior in similarly overaged 2124 alloy. Overaging in 2090, which led to decreases in strength and toughness principally through the formation of plate-like copper-rich grain boundary precipitates and associated copper-depleted and δ' precipitate-free zones, was found to result in increased fatigue crack growth rates above $\sim 10^{-9}$ m/cycle; near-threshold growth rates were less affected. Such behavior is related to a diminished role of crack-tip shielding during crack extension in overaged microstructures, from less crack deflection and lower crack closure levels (from asperity wedging), arising from more linear crack paths. Despite this degradation in fatigue crack growth properties following high temperature exposure, crack growth rates in the overaged 2090 remain comparable or superior to traditional high strength aluminum alloys, such as 2124-T351 and 7150-T651, due primarily to higher overall levels of crack-tip shielding.

1. INTRODUCTION

Due principally to their lower density, higher strength and stiffness, and superior fatigue and cryogenic toughness properties compared to traditional high strength aluminum alloys (1-4), aluminum-lithium alloys have recently been targeted for potential use in advanced aerospace vehicles, such as the Advanced Tactical Fighter and the National Aerospace Plane. With certain components, such applications will involve periodic exposures to high temperatures for prolonged time periods during service, which potentially may degrade the mechanical properties of the alloy through overaging. Although extensive data have recently been documented on the effect of such thermal conditions on tensile properties (5), little information exists on toughness and fatigue properties. It is thus the purpose of this paper to examine the effect of such high-temperature exposures (up to 1000 hr at 163°C) on the microstructure, fracture and fatigue resistance of a commercial Al-Li-Cu-Zr alloy, 2090-T8E41, and to compare behavior to a similarly overaged 2124 aluminum alloy.

2. EXPERIMENTAL PROCEDURES

Aluminum-lithium alloy, 2090, was received from ALCOA as commercially peak-aged (T8E41) 12.7 mm thick plate. The designation T8E41 refers to a solution treatment at 549°C, water quench, and 6% stretch prior to aging 24 hr at 163°C (6). The alloy was compared with a similar-sized plate of 2124-T351. Compositions are listed in Table 1. Prolonged high-temperature exposures were carried out by

further aging at 163°C (325°F) for 100 and 1000 hr to yield lightly overaged (LOA) and highly overaged (OA) microstructures, respectively. Corresponding room temperature mechanical properties are listed in Table 2.

TABLE 1

Composition of aluminum alloys 2090 and 2124

Element amount (wt.%)	Cu	Li	Zr	Cr	Zn	Fe	Si	Mg	Mn	Ti	Al
2090	2.86	2.05	0.12	-	-	0.02	0.01	0.01	0.005	0.02	bal
2124	4.50	-	-	0.10	0.25	0.30	0.20	1.50	0.500	0.15	bal

TABLE 2

Room temperature mechanical properties of aluminum alloys 2090 and 2124 as a function of aging treatment

Alloy	Yield strength (MPa)	Tensile strength (MPa)	Elongation in 14 mm (%)	Fracture toughness ($MPa\sqrt{m}$)
2090-T8E41	548	579	9.3	24
2090 LOA	545	566	12.0	-
2090 OA	466	527	10.0	20
2124-T351	360	488	17.8	-
2124 LOA	474	505	10.7	42
2124 OA	432	477	8.4	45

Fracture toughness, K_{IC}, and (long-crack) fatigue crack propagation testing were performed in room temperature air (22°C, 45% relative humidity) on 6.7 mm thick compact C(T) specimens, machined from the central sections of the plates in the T-L orientation. Constant-amplitude crack growth tests were conducted along the guidelines of the ASTM standard E 647-86A (7), using automated electro-servo-hydraulic testing machines, operating at a frequency of 50 Hz (sine wave) with a load ratio (K_{min}/K_{max}) of 0.1. An exponential load shedding scheme, using a normalized stress-intensity K-gradient of -0.1 mm^{-1} (7), was used to measure near-threshold growth rates; fatigue thresholds, ΔK_{TH}, being defined operationally (11) at a maximum growth rate of 10^{-12} m/cycle. Crack length and crack closure were continuously monitored using d.c. electrical potential and back-face strain compliance techniques, respectively. The closure stress intensity, K_{cl}, was measured at first deviation from linearity of the unloading compliance curve, corresponding to first contact of the fracture surfaces (8). Crack growth data are thus described in terms of both the nominal ($\Delta K = K_{max} - K_{min}$) and effective ($\Delta K_{eff} = K_{max} - K_{cl}$) stress intensity ranges.

Fracture toughness and fatigue fracture surfaces were examined in the scanning electron microscope (SEM) and from crack path profiles, obtained by metallographic sectioning at specimen center-thickness, normal to the fracture surface, on cracks previously impregnated with epoxy.

3. RESULTS

Microstructure

In the as-received T8E41 condition, 2090 shows a highly anisotropic, unrecrystallized microstructure, with large pan-cake shaped grains (~ 20 μm thick by 500 μm wide), elongated several mm in the rolling direction (Fig. 1). Using transmission electron microscopy, it is evident that strengthening in the peak aged condition is due to coherent, ordered, spherical precipitates of δ' (Al_3Li), and plate-like precipitates T_1' (Al_2CuLi) and T_2' (Al_5CuLi_3), together with β' (Al_3Zr) dispersoids (Fig. 2a), as has been described elsewhere (6,9). Precipitates are generally distributed homogeneously within the grains, and are largely suppressed on grain boundaries due to the 6% stretch prior to artificial aging.

Recrystallization or grain growth was not observed during overaging, even for 1000 hr exposures. However, there was evidence of coarsening of the matrix δ', T_1' and T_2' precipitates, an increased density of possibly T_1' or T_2' along subgrain boundaries, and the formation of δ and copper-rich plate-like precipitates along grain boundaries, resulting in copper-depleted and δ' precipitate-free zones (PFZs) (Fig. 2b), similar to results reported for experimental Al-Li-Cu alloys (10).

Strength and Toughness Properties

Whereas 100 hr overaging treatments on 2090 produced only a negligible change in mechanical properties compared to the T8E41

condition, both yield strength and toughness were reduced roughly 15% following overaging for 1000 hr (Table 2). Corresponding results for 1000 hr overaged 2124 show a 20% increase in strength and a marginal increase in toughness, compared to the T351 temper.

Fracture surfaces of the toughness specimens in 2090 are shown in Fig. 3, and indicate predominantly intergranular fracture (intergranular bands run parallel to the crack growth (rolling) direction), interdispersed with regions of microvoid coalescence. With increased aging times, the lower toughness is associated with a more pronounced intergranular mode, consistent with the enhanced grain and subgrain boundary precipitation and corresponding PFZs (Fig. 2b). In addition, there is evidence of void coalescence around 1 to 2 μm sized iron- and copper-rich intermetallic particles.

Fatigue Crack Growth Behavior

Fatigue crack propagation and associated levels of crack closure for the peak-aged (T8E41) and two overaged microstructures in alloy 2090 are shown as a function of the nominal ΔK in Fig. 4. It is apparent that, while near-threshold growth rates and the value of ΔK_{TH} remain relatively unaffected, with increasing overaging crack propagation rates above $\sim 10^{-9}$ m/cycle become progressively faster, by up to an order of magnitude (Fig. 4a).

The accelerated growth rates in the overaged structures are concurrent with decreased closure levels (Fig. 4b), consistent with a change in crack path morphology (Fig. 5). As reported elsewhere

(11,12), fatigue crack paths in the T8E41 microstructure show significant microscopic deflection and macroscopic branching/meandering (i.e., general crack path tortuosity), due primarily to the intense slip planarity and strong texture, respectively (Fig. 5a). These factors provide a potent means of lowering the **local** "crack driving force" experienced at the tip, i.e., a reduced ΔK_{eff} through crack tip shielding (8), from such mechanisms as crack deflection (13) and resulting roughness-induced crack closure (14-16) from the wedging action of enlarged asperities inside the crack. With prolonged overaging, crack paths ultimately become macroscopically linear (Fig. 5c), accounting for the lower closure levels and faster growth rates (Fig. 4).

Representative SEM fractographs of fatigue surfaces in 2090 are shown in Fig. 6. It is apparent that the well-defined transgranular facets characteristic of heavily deflected crack paths in the peak-aged condition become "smoothed out" in the overaged structures. In addition, there is increasing evidence of surface oxidation on the overaged fatigue fracture surfaces. Mean excess oxide thicknesses (17), measured using Auger spectroscopy, were found to be of the order of 2 to 10 nm in these microstructures. Such deposits, however, were considered unlikely to promote significant oxide-induced crack closure (18,19), as their size was small compared to cyclic and maximum crack tip opening displacements (i.e., which were of the order of 50 and 150 nm, respectively, at ΔK_{TH}).

4. DISCUSSION

Overaging in traditional high-strength aluminum alloys, such as 2024, 7075, etc., generally yields microstructures strengthened by incoherent matrix and grain boundary precipitates, with associated PFZs and decreased slip planarity. Compared to peak-aged conditions, such microstructures show lower strength yet comparable, if not improved, toughness (e.g., 2124 results in Table 2), due largely to a change from planar to dispersed slip (e.g., ref. 20). Aluminum-lithium alloy 2090, conversely, shows a reduction ($\sim$ 15%) in strength and toughness on overaging (see also ref. 5), similar to that reported for experimental Al-Li-Cu-Zr alloys containing 2 to 3 wt% Li (21,22). Whereas decreased slip planarity, which results in a reduced propensity for crack bifurcation and branching, has been suggested as one mechanism for decreasing toughness with aging (23)*,

---

*Decreasing slip planarity is generally considered to increase toughness, as planar slip can lead to strain localization at grain boundaries, thereby enhancing the formation of microcracks or voids at grain boundary precipitates (20,24-26).

---

no evidence was found for major geometrical changes in crack path in toughness tests of 2090, based on metallographic sectioning taken at specimen mid-thickness. Conversely, the lower toughness on overaging appears to be associated primarily with grain boundary precipitation and resulting strain localization in weak, solute-depleted precipitate-free zones and a decreased volume fraction of strengthening precipitates. It is thus apparent that the

commercially peak-aged T8E41 microstructure offers optimum mechanical properties, at least with respect to strength and toughness.

With respect to fatigue crack propagation, the T8E41 microstructure similarly displays optimum properties. This has been attributed primarily to the deflected and branched nature of the fatigue crack paths, which result from the marked slip planarity and strong texture in this microstructure (11,12). This in turn promotes significant crack tip shielding, primarily from mechanisms of crack deflection and consequent crack closure from asperity wedging. With prolonged overaging, however, crack growth properties are clearly degraded, although the magnitude of the effect is not large and predominates above $\sim 10^{-9}$ m/cycle (Fig. 4). From Figs. 4 and 5, it is evident that the faster growth rates are directly associated with lower crack closure levels, concomitant with a decreasing tendency for crack path tortuosity, and lower slip reversibility, from the more dispersed nature of slip in the overaged microstructures.

Despite losses in strength, toughness and fatigue resistance with prolonged exposure at 163°C, the properties of overaged 2090 remain comparable, if not superior, to similarly overaged traditional high-strength aluminum alloys in all but (ambient temperature) fracture toughness. For example, overaged 2090 displays similar strength, far superior fatigue crack growth rate behavior below $\sim 10^{-9}$ m/cycle (with a 50% higher fatigue threshold), and identical behavior above 10^{-9} m/cycle to peak-aged and overaged 2124 alloys

(Fig. 7a). Essentially, the linear crack paths induced by overaging in 2090 reduce the measured closure levels to that of 2124 (Fig. 7b). In addition, the overaged alloy compares favorably with the growth-rate behavior of commercially heat-treated alloys; it is comparable to 2124-T351 and and 7150-T651, and is superior to that of 7150-T751 (Fig. 8).

Finally, it should be noted that since the beneficial fatigue crack propagation properties of 2090 result in large part from enhanced crack tip shielding due to deflected crack paths (promoted by marked slip planarity and texture), the superior crack growth resistance may not be retained where principal mechanisms of shielding are restricted. This has been observed in the 2090-T8E41 alloy at high load ratios, where the larger crack opening displacements minimize the effect of crack closure induced by wedging of asperities (12); in the presence of periodic compression overload cycles, where the compressive stresses can reduce closure by crushing such asperities (11); and with microstructurally and physically ($\lesssim$ 1 mm) small cracks, where the diminished crack wake markedly limits the development of all closure mechanisms (27).

5. CONCLUSIONS

Based on a study on the effects of 100 and 1000 hr overaging exposures at 163^{o}C on the fatigue and fracture behavior of commercially peak-aged 12.7 mm thick plate of Al-Li-Cu-Zr alloy 2090-T8E41, the following conclusions can be drawn:

1. Whereas only negligible changes in mechanical properties were detected following 100 hr overaging exposures, 1000 hr exposures were found to induce $\sim$ 15% reductions in yield strength and fracture toughness, compared to the peak-aged condition. Such degradation in strength and toughness on overaging was attributed to the coarsening of matrix precipitates (δ', T_1', T_2'), and the formation of subgrain boundary T_1' or T_2' precipitates and grain boundary δ and Cu-rich precipitates, which resulted in Cu-depleted and precipitate-free zones.

2. Above $\sim 10^{-9}$ m/cycles, fatigue crack growth rates progressively increased with prolonged overaging, although near-threshold growth rates below $\sim 10^{-9}$ m/cycle were comparatively unchanged. Such behavior was attributed to a measured reduction in crack closure in overaged, compared to peak-aged, microstructures, consistent with a macroscopic change from branched to linear crack paths, associated with decreased slip planarity.

3. Despite reductions in strength and fatigue resistance following 1000 hr exposures at 163°C, fatigue crack growth rates in overaged 2090 are still comparable, if not superior, to similarly overaged 2124 alloys, and to commercially heat-treated 2124-T351, 7150-T651 and 7150-T751 alloys.

ACKNOWLEDGEMENTS

This work was supported by the Director, Office of Energy Research, Office of Basic Energy Sciences, Materials Sciences

Division of the U.S. Department of Energy under Contract No. DE-AC03-76SF00098. The authors are grateful to Dr. P. E. Bretz of ALCOA for provision of the alloys, and to Drs. G. V. Scarich, G. R. Chanani and K. M. Bresnahan of Northrop for suggesting the study. In addition, thanks are due to Drs. R. J. Bucci, R. R. Sawtell and W. Quist for many helpful discussions, and to Dr. Weikang Yu, Lai Hing Chan, Hiro Hayashigatani and Leela Gill for experimental assistance.

REFERENCES

1 T. H. Sanders and E. A. Starke (eds.), Aluminum-Lithium Alloys, TMS-AIME, Warrendale, PA, 1981.

2 T. H. Sanders and E. A. Starke (eds.), Aluminum-Lithium Alloys II, TMS-AIME, Warrendale, PA, 1983.

3 C. Baker, P. J. Gregson, S. J. Harris, and C. J. Peel (eds.), Aluminium-Lithium Alloys III, Institute of Metals, London, U.K., 1986.

4 J. Glazer, S. L. Verzasconi, E. N. C. Dalder, W. Yu, R. A. Emigh, R. O. Ritchie, and J. W. Morris, Advances in Cryogenic Engineering, 32 (1986) 397.

5 R. C. Malcolm, F. J. Cordier, and R. J. Bucci, "The Effects of Various Thermal Conditions on the Tensike Properties of Aluminum Alloy 2090-T8E41 Plate (0.500-inch Thick)", Alcoa Alloy Tech. Div. Report No. 56-86-AH429, Aluminum Company of America, Oct. 1983

6 R. J. Rioja, P. E. Bretz, R. R. Sawtell, W. H. Hunt, and E. A. Ludwiczak, in E. A. Starke and T. H. Sanders (eds.), Aluminum Alloys: Their Physical and Mechanical Properties, EMAS Ltd., Warley, U.K., 1986.

7 ASTM Standard E 647-86A, "Standard Test Method for Constant Amplitude Fatigue Crack Growth Rates", in 1986 ASTM Annual Book of Standards, vol. 3.01, American Society for Testing and Materials, Philadelphia, PA, 1986.

8 R. O. Ritchie and W. Yu, in R. O. Ritchie and J. Lankford (eds.), Small Fatigue Cracks, TMS-AIME, Warrendale, PA, 1986, p. 167.

9 R. J. Rioja and E. A. Ludwiczak, in ref. 3, p. 471.

10 C. Kumai, J. Kusinski, G. Thomas, and T. M. Devine, Corrosion, 1987, in review.

11 W. Yu and R. O. Ritchie, J. Eng. Matls. Tech., Trans. ASME, Series H, 109 (1987) 81.

12 K. T. Venkateswara Rao, W. Yu, and R. O. Ritchie, Metall. Trans. A, 18A (1986) in review.

13 S. Suresh, Metall. Trans. A, 14A (1983) 2375.

14 N. Walker and C. J. Beevers, Fat. Eng. Mat. Struct., 1 (1979) 135.

15 K. Minakawa and A. J. McEvily, Scripta Metall., 6 (1981) 633.

16 S. Suresh and R. O. Ritchie, Metall. Trans. A, 13A (1982) 1627.

17 S. Suresh and R. O. Ritchie, Scripta Metall., 17 (1983) 575.

18 A. T. Stewart, Eng. Fract. Mech., 13 (1980) 463.

19 R. O. Ritchie, S. Suresh, and C. M. Moss, J. Eng. Matls. Tech., Trans. ASME, Series H, 102 (1980) 293.

20 G. G. Garrett and J. F. Knott, Metall. Trans. A, 9A (1978) 1187.

21 K. V. Jata and E. A. Starke, Metall. Trans. A, 17A (1986) 1011.

22 S. Suresh, A. K. Vasudévan, M. Tosten, and P. R. Howell, Acta Metall., 35 (1987) 25.

23 A. K. Vasudévan and S. Suresh, Mater. Sci. Eng., 72 (1985) 37.

24 B. Noble, S. J. Harris, and K. Dinsdale, Metal. Sci., 16 (1982) 425.

25 T. H. Sanders and E. A. Starke, Acta Metall., 30 (1982) 927.

26 P. J. Gregson and H. M. Flower, Acta Metall., 33 (1985) 527.

27 K. T. Venkateswara Rao, W. Yu, and R. O. Ritchie, Scripta Metall., 20 (1986) 1459.

28 E. Zaiken and R. O. Ritchie, Mater. Sci. Eng., 70 (1985) 151.

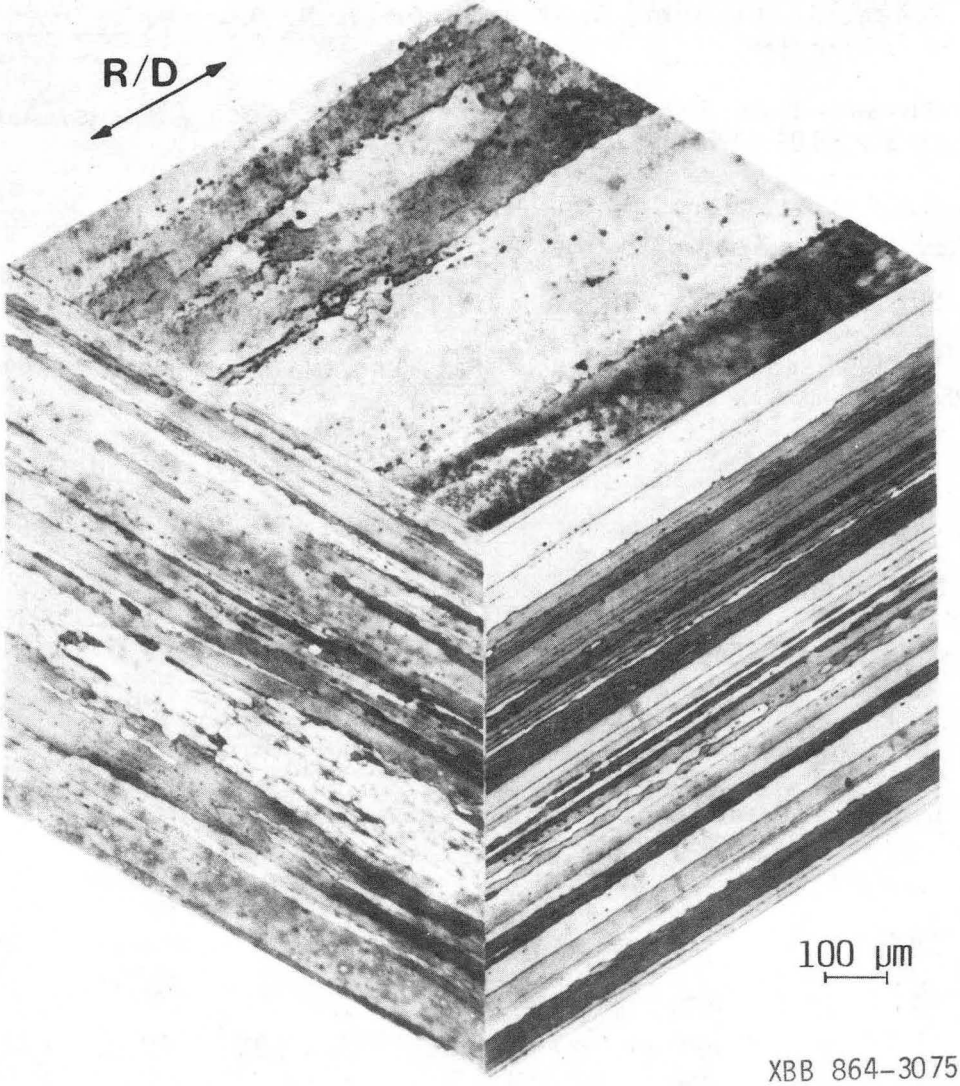

Fig. 1. Three-dimensional optical metallograph of the pancake-shaped grain structure of 12.7 mm thick plate of Al-Li-Cu-Zr alloy 2090-T8E41 (Keller's reagent etch).

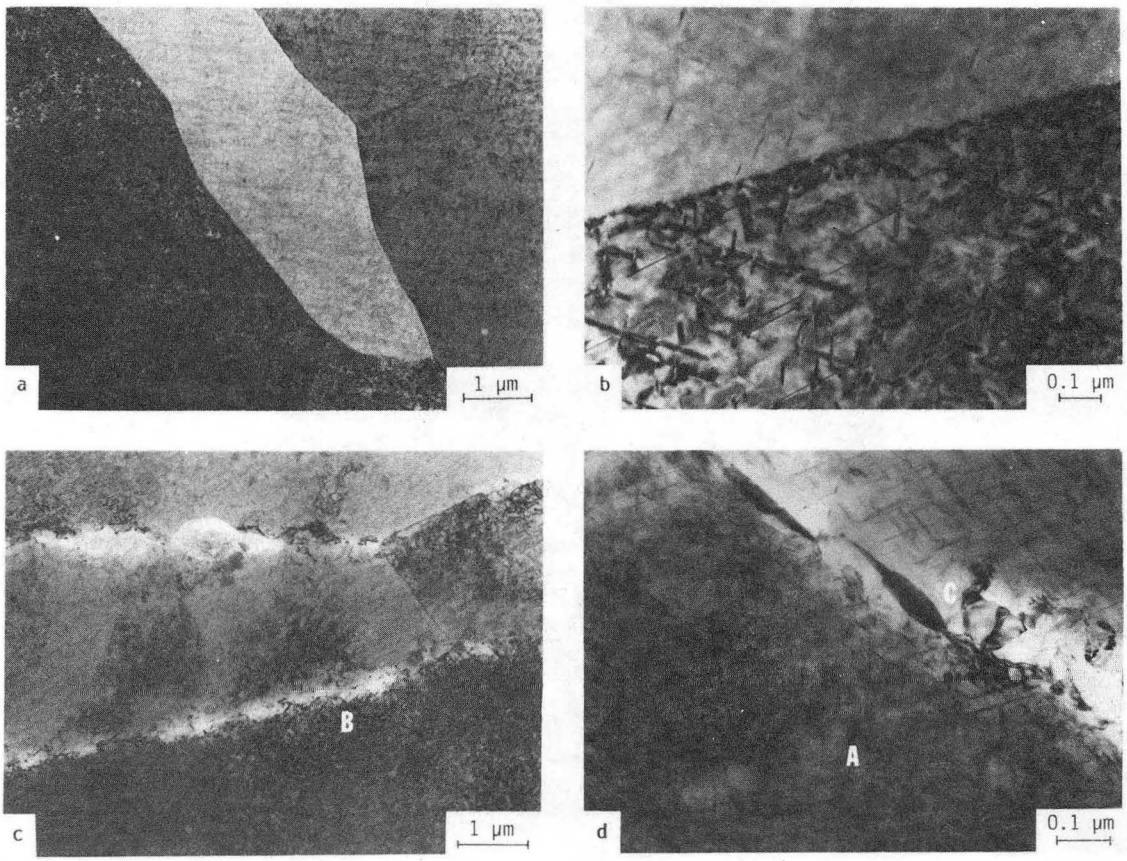

Fig. 2. Transmission electron micrographs of microstructures in the Al-Li-Cu-Zr alloy 2090 in a) b) peak-aged (T8E41) condition, and c) d) overaged (~1000 hours at 163°C) condition. Prolonged aging results in coarsening of matrix precipitates δ', T_1', T_2' (see region A), subgrain boundary and grain boundary precipitation of δ and Cu-rich precipitates (regions B and C) and the consequent formation of precipitate-free zone (see text).

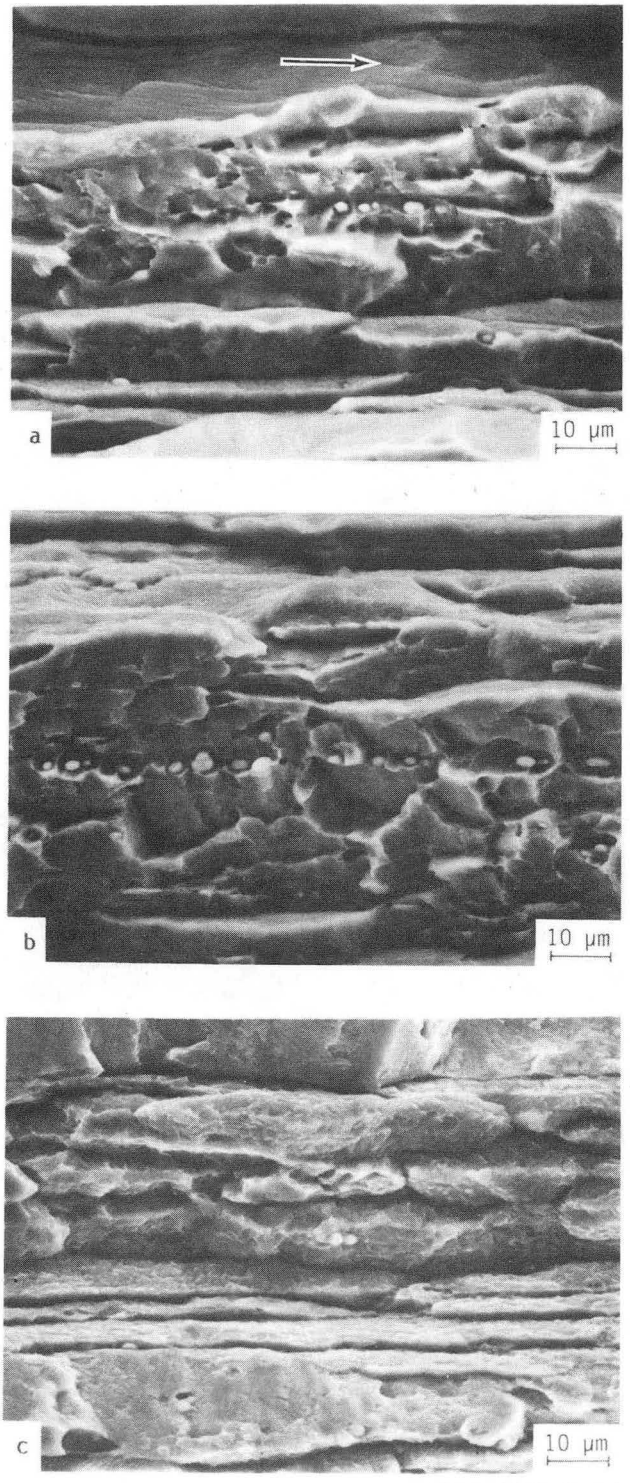

XBB 874-2891

Fig. 3. Scanning electron micrographs showing predominantly intergranular fracture associated with toughness tests in alloy 2090 in a) peak-aged (T8E41), b) ~100 hr overaged (L0A), and c) ~1000 hr overaged (0A) conditions. Note evidence of void coalescence around 1 to 2 μm particles, which were identified as Fe/Cu-rich intermetallics. Arrow indicates general direction of crack growth.

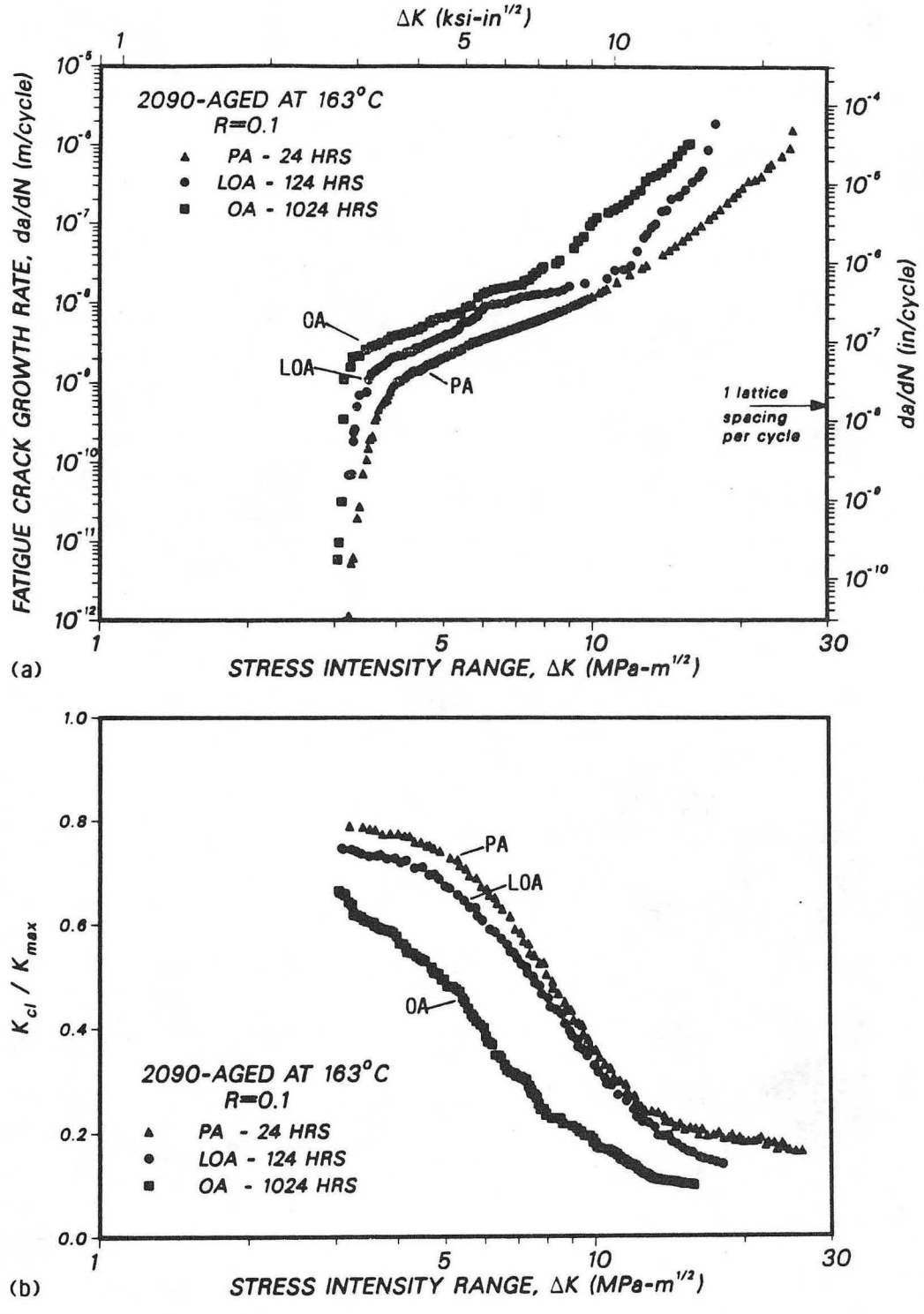

Fig. 4. Variation in a) fatigue crack growth rates (da/dN) and b) crack closure (K_{cl}) levels at R = 0.1 in 2090 alloy in the peak-aged (T8E41), lightly overaged (LOA) and overaged (OA) conditions. Note the increase in crack growth rates (particularly above $\sim 10^{-9}$ m/cycle), concomitant with lower closure levels, with prolonged overaging.

XBL 876-2523

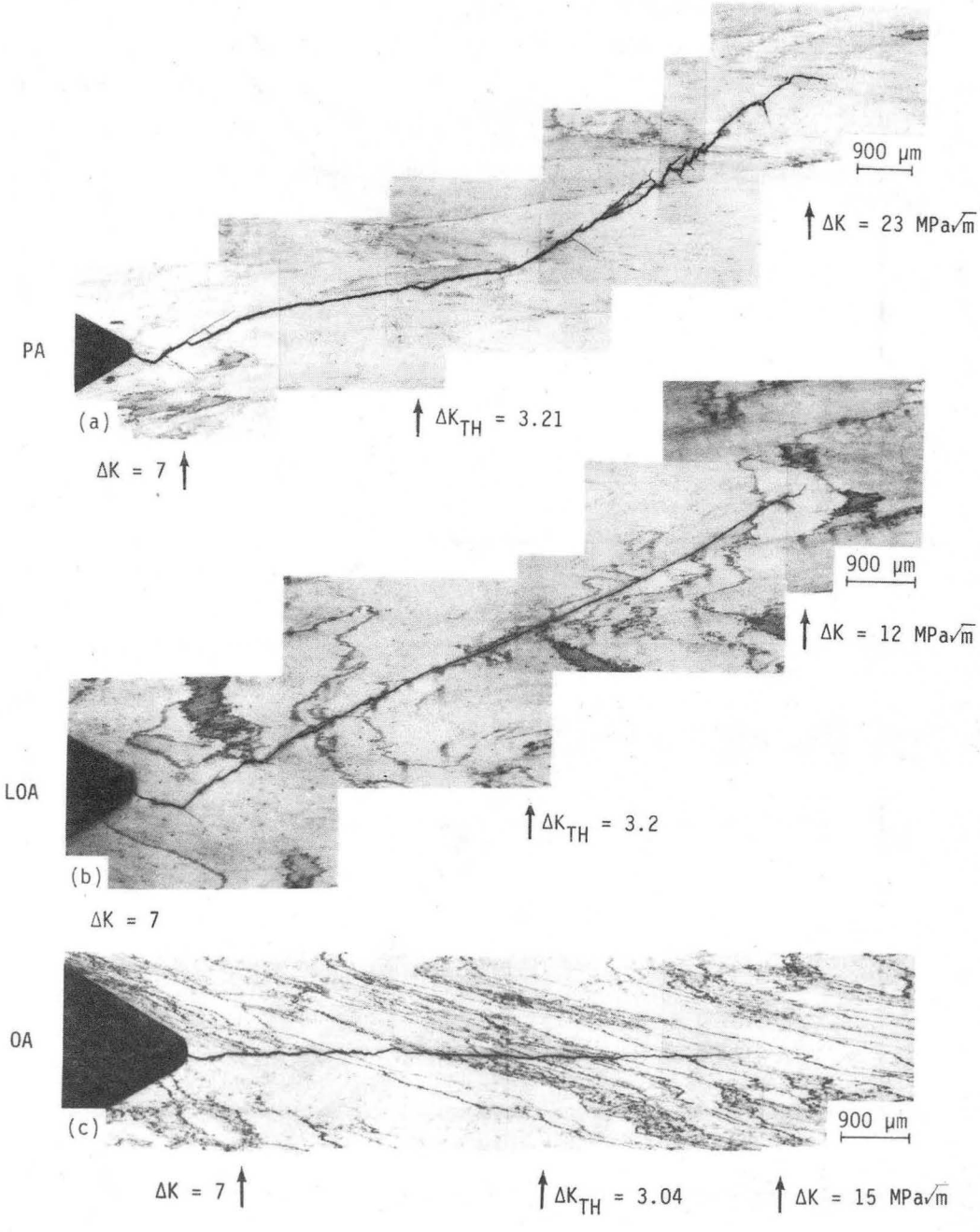

Fig. 5. Optical micrographs of the morphology of fatigue crack paths in 2090 alloy, showing a,b) branched and meandering cracks typical of the peak-aged (T8E41) and ~100 hr overaged (LOA) microstructures, and c) linear crack profiles typical of the ~1000 hr overaged (OA) microstructures (Keller's reagent etch).

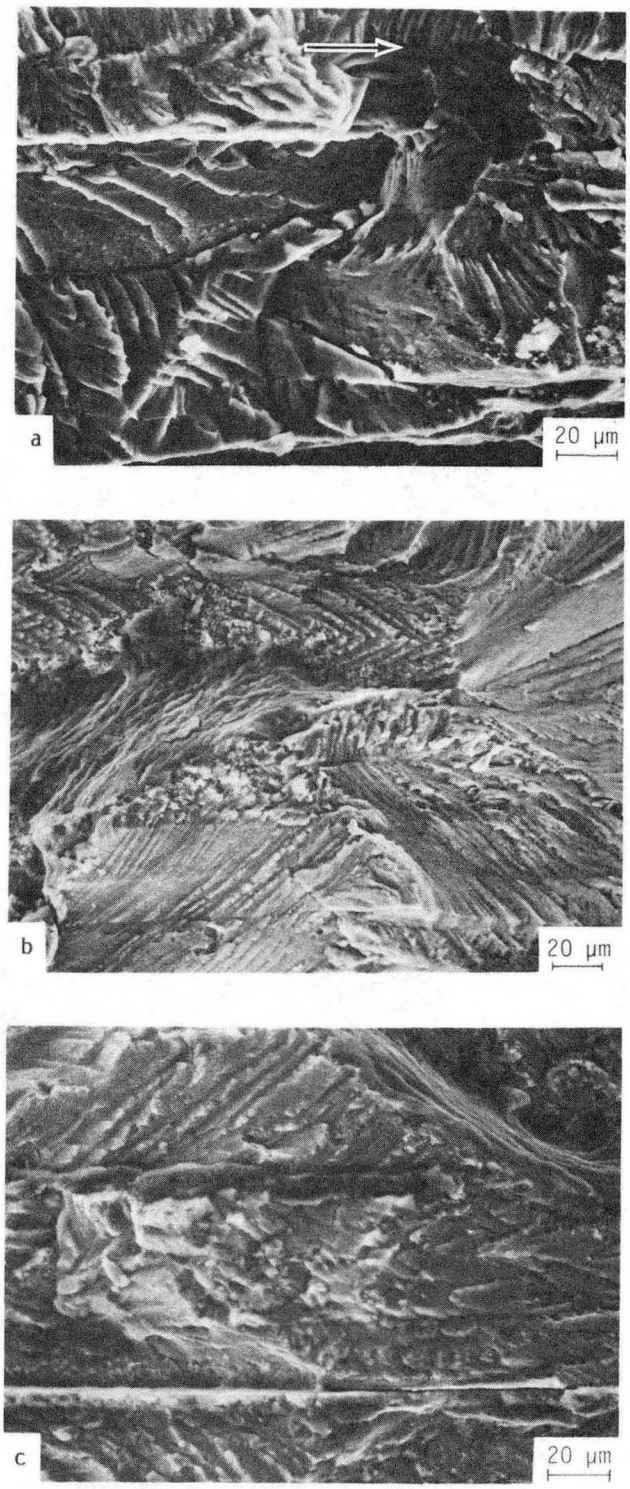

XBB 874-2892

Fig. 6. Scanning electron micrographs of near-threshold fatigue fracture surfaces in 2090 alloy at ΔK = 3 – 8 MPa $\sqrt{m}$ (R = 0.1) for a) peak-aged (T8E41), b) ~100 hr overaged (L0A), and c) ~1000 hr overaged (0A) microstructures. Note how fatigue fractures are transgranular compared to predominantly intergranular fracture in toughness tests (Fig. 3). Arrow indicates the general direction of crack growth.

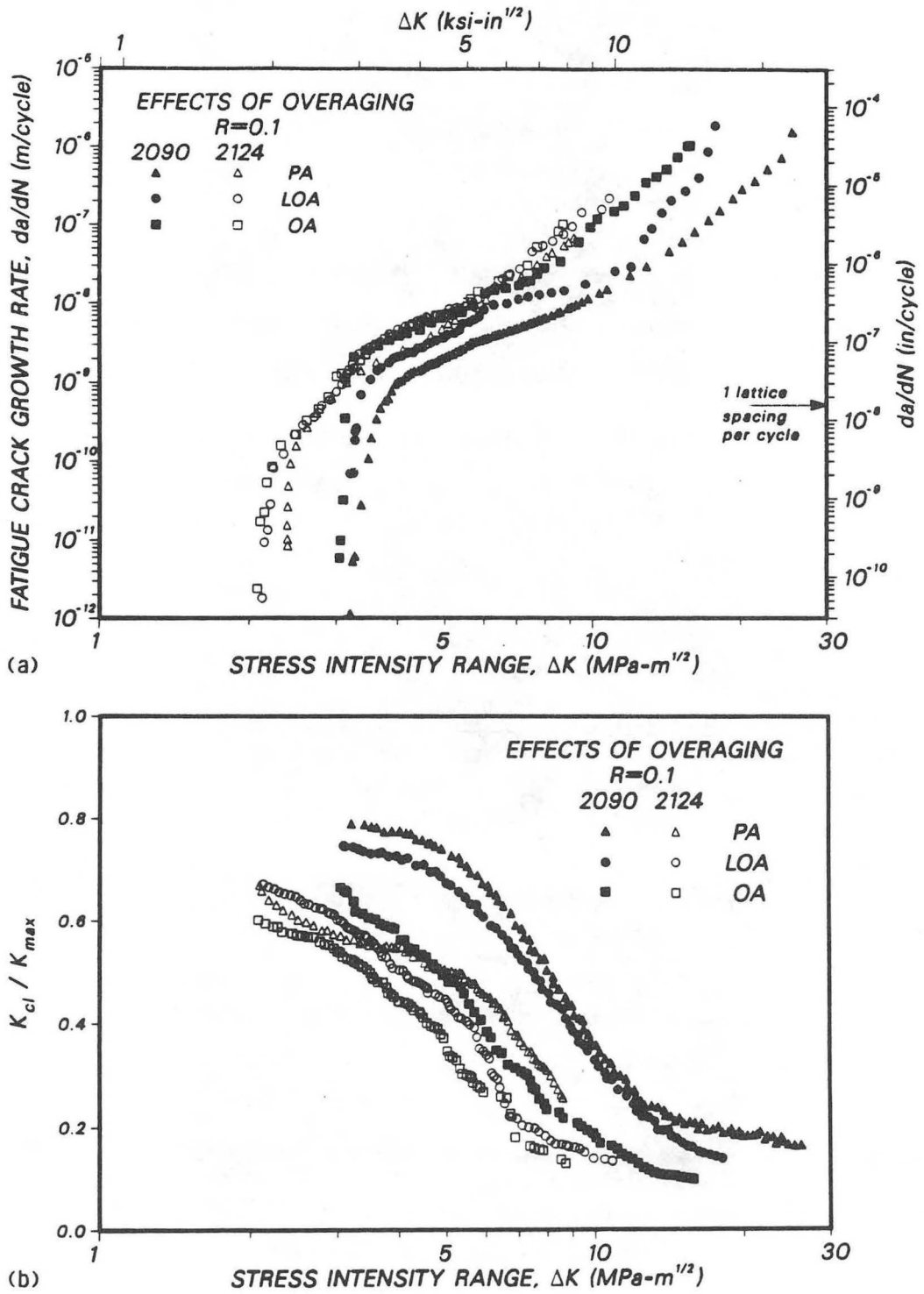

Fig. 7. Comparison of a) fatigue crack propagation rates (da/dN), and b) crack closure (K_{cl}) behavior at R = 0.1 in 2090 and 2124 alloys (T-L orientation) subjected to ∿ 100 hr and ∿ 1000 hr exposures at 163°C.

XBL 876-2524

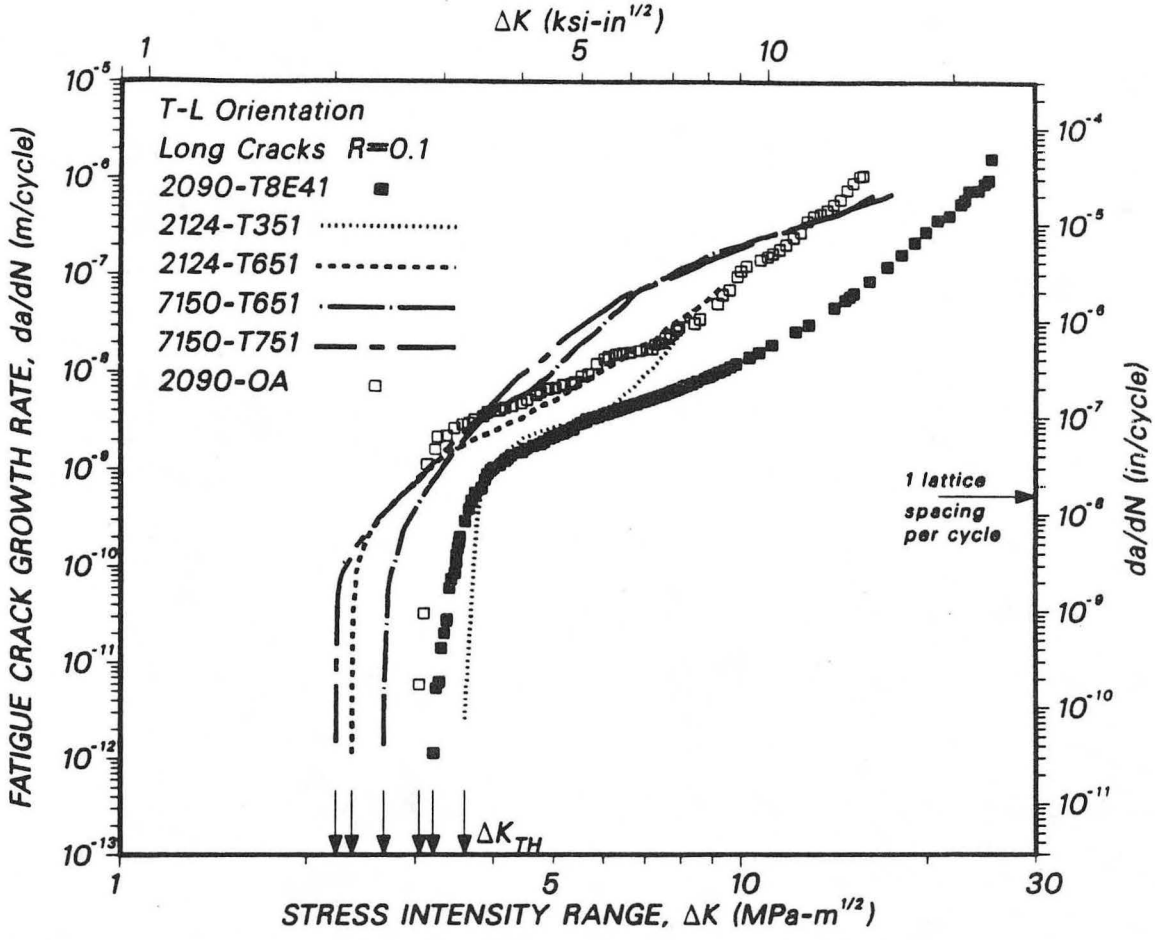

Fig. 8. Comparison of the fatigue crack propagation behavior of peak-aged (T8E41) and overaged (1000 hr at 163°C) 2090 alloy with published results for 2124-T351, 7150-T651 and 7150-T751. Note how 2090, even after 1000 hr overaging exposures, remains comparable, if not superior, to traditional high strength aluminum alloys. Data for 2124 and 7150 were taken from refs. 8 and 28.

XBL 876-2525

LAWRENCE BERKELEY LABORATORY
TECHNICAL INFORMATION DEPARTMENT
UNIVERSITY OF CALIFORNIA
BERKELEY, CALIFORNIA 94720